Structural reordering in monolayers of gold nanoparticles during transfer from water surface to solid substrate

R. Banerjee,[1] M. K. Sanyal,[1] M. K. Bera,[1] A. Singh,[2] J. Novak,[2] and O. Konovalov[2]
[1]*Surface Physics Division, Saha Institute of Nuclear Physics, 1/AF Bidhannagar, Kolkata 700 064, India*
[2]*European Synchrotron Radiation Facility, Beamline ID10B, P. O. Box 220, F-38043 Grenoble, France*
(Received 31 January 2011; published 16 May 2011)

Structural reordering in monolayers of gold nanoparticles during transfer from water surface to solid substrate has been studied by synchrotron x-ray scattering techniques. Grazing incidence diffraction (GID) and grazing incidence x-ray off-specular scattering (GIXOS) measurements were performed as a function of time to track the in-plane and out-of-plane structural reordering in the transferred monolayers. GID measurements show shift in the in-plane particle-particle correlation peak toward the lower in-plane momentum transfer value, signifying possible expansion of triangular lattice formed on the water surface. However, GIXOS data and supportive microscopy measurements clearly show compactification in the in-plane structure and associated out-of-plane movements. A model that assumes the possibility of a two-dimensional short-range structural reordering from triangular to square-like lattice as a function of time could explain all the data. The observed change in the electron densities of the nanoparticles before and after the structural reordering matches well with the expected change in the calculated electron densities of the nanoparticles arranged in triangular (pretransition) and square-like (post-transition) symmetry.

DOI: 10.1103/PhysRevE.83.051605 PACS number(s): 68.47.Pe, 64.70.Nd, 61.05.cf

I. INTRODUCTION

Structural reordering in solids proceeds via complicated phases covering a range of stable and metastable configurations [1]. Detailed investigations have revealed that the thermodynamic properties guiding the evolution and phase stability of nanostructures are distinctly different from their bulk counterparts [2,3]. Ordering and dynamics of self-assembling colloidal nanosystems leading to morphological and/or structural transitions in two dimensions is governed by the growth equations [4] as well as the experimental parameters associated with the process and has propelled research activities with the advent of state-of-the-art techniques like scattering and microscopy. Self-assembling processes are universal in nature, and a lot of materials with vastly different physical properties are known to self-assemble in a very similar fashion [5]. The understanding and control of such mechanism promises implementation of smart technologies in nanodevice fabrication. It is known that during the self-assembling processes of colloidal systems like thiol-encapsulated gold nanoparticles, internal stress is generated by drying/dewetting forces as well as the underlying interfacial interactions [6], which induces patterning in monolayers of such colloids when transferred over solid substrate [7–9].

Thiol-encapsulated gold nanoparticles have been known to posses unique structural [10], electrical [11–13], optical [14], and magnetic properties [15] and are competent candidates for fabrication of modern miniature devices. Recent investigations have shown pattern formation by tracking the evolution in the structure of transferred monolayer of gold nanoparticles by time-resolved x-ray reflectivity (XRR) and atomic force microscopy (AFM) measurements [3]. The monolayer exhibited an instability in structure immediately after transfer and systematic XRR and AFM measurements gave insight into the gross in-plane and out-of-plane morphological restructuring induced by drying/dewetting forces. However, to the best of our knowledge, microscopic details about the structural reordering in the transferred monolayer as a function of drying time has not been probed so far. Various synchrotron x-ray scattering techniques, such as grazing incidence diffraction (GID) and grazing incidence x-ray off-specular scattering (GIXOS), have been used extensively to study both in-plane and out-of-plane structure of monolayers of fatty acids [16] and nanoparticles on water surface [10,17]. In this paper, we report the results of *in situ* GID and GIXOS measurements on a monolayer of gold nanoparticles transferred from an air-water interface to a Silicon substrate. The results obtained from scattering and microscopy measurements of the transferred monolayer is consistent with an in-plane structural reordering from triangular (Δ) to square($\square$)-like lattices.

It is known that colloidal nanosystems are prone to structural phase transitions under the influence of external parameters such as temperature [18,19], confinement [1,20,21], shear [22,23], and electrical and magnetic fields [24–26]. Structural phase transitions and/or restructuring in colloidal systems have been probed by reflectance spectroscopy [27] and *in situ* GID measurements [28]. Sequence of structural transformation from $n\Delta \rightarrow (n+1)\square \rightarrow (n+1)\Delta$ of such colloidal systems when trapped within optically flat, wedge-like surfaces have been observed with increasing separation between the surfaces [29,30]. Here, n is the number of layers, and Δ and $\square$ are layers corresponding to triangular and square symmetry, respectively. In our present system, n is 1 since we are dealing with monolayers of gold nanoparticles that tend to form an overlayer as a function of time during the process of transfer from water to a solid surface. For small n, the sequence of structural reordering is expected to become continuous following the transition $1\Delta \rightarrow 1\mathrm{B} \rightarrow 2\square$, where B is the buckled phase [31]. On the basis of scattering and supportive microscopic measurements, we propose that the two-dimensional (2D) structure of the gold nanoparticles undergoes similar structural reordering, wherein the 2D Δ or hexagonal ordering gradually assumes a buckled phase and

 ©2011 American Physical Society

is then rearranged into a 2D □-like ordering as a function of time.

II. EXPERIMENTAL

Thiol-encapsulated gold nanoparticles were synthesized by the method of Brust *et al.* [32]. The metallic core of average diameter was determined to be 2.9 ± 0.55 nm by transmission electron microscopy (TEM) measurements [3]. The thiol-encapsulated gold nanoparticles used in our experiments are neutral. Generally, gold nanoparticles are produced by "liquid chemical methods" (the Brust Method in our case) by reduction of chloroauric acid ($H[AuCl_4]$). After dissolving $H[AuCl_4]$, the solution is rapidly stirred while a reducing agent is added. This causes Au^{3+} ions to be reduced to neutral gold atoms. As more and more of these gold atoms form, the solution becomes supersaturated, and gold gradually starts to precipitate in the form of subnanometer particles. Such nanoparticles are known to show unique electronic [11–13] and magnetic properties [15] at low temperatures. However, here we have carried out all our measurements at room temperature (20°C) and assumed that long-range forces like electrical and magnetic forces is not affecting the monolayer structure. About 200 μL aliquot of the solution containing nanoparticles in toluene at a concentration of 10^{15} nanoparticles/mL (or 0.44 mg/mL) was spread on a Langmuir trough (KSV Minimicro), placed on an antivibration device over the spectrometer, and a pressure-area isotherm was recorded at 20 °C.

The x-ray scattering experiments were performed on a liquid spectrometer at ID 10B beamline at the European Synchrotron Radiation Facility (ESRF) in Grenoble, using a high-energy (8 KeV, $\lambda = 1.54$ Å) synchrotron source. To facilitate measurements from the transferred film of nanoparticle on a substrate, a bare hydrophillized Si substrate mounted on the dipper unit of the Langmuir trough was aligned with respect to the incident x-ray beam. The prealignment ensured that once the monolayer is transferred, the measurements could be performed instantaneously. After the alignment, the substrate was submerged below the air-water interface and the aliquot was spread carefully on the water surface. Once the toluene evaporated, the barriers were compressed slowly (at a speed of 1 mm/min) to attain a target pressure of 3 mN/m much below the collapse of the monolayer to a bilayer. A slow compression speed (1 mm/min or less) is always desirable for the formation of compact monolayers of gold nanoparticles in the Langmuir trough. Faster compression rates make the monolayer susceptible to premature collapse and/or aggregation of the nanoparticles, since the energy required for a gold nanoparticle to flip up and form a bilayer is only k_BT. All isotherm measurements, as well as sample transfer, have been carried out at slower compression speed. On achieving the target pressure, scattering measurements were performed on the monolayer of nanoparticles at the air-water interface. The monolayer was then transferred to the substrate at the same pressure by the horizontal deposition technique [3,33], and scattering measurements were performed repeatedly at frequent intervals of time during the drying process of the transferred monolayer on the substrate.

The scattered intensity from the monolayer was collected from water surface/Si substrate, as a function of in-plane (ϕ) and out-of-plane (θ_f) angles, by using a linear position sensitive detector (PSD). Incident angle (θ_i) for all measurements on water surface as well as Si substrate were fixed at 0.13°, which is less than the critical angles (θ_c) for both water (0.15°) and Si (0.22°) at this energy. Low angle of incidence ensured that the scattering information obtained is primarily from the surface due to low penetration of x-rays below the critical angle. The scattered intensities were then plotted as function of in-plane and out-of-plane components ($q_\parallel$, q_z) of the momentum transfer vector ($\vec{q}$), which are related to the in-plane and out-of-plane angles, respectively [10,34], as shown in Fig. 1. GID patterns (which provide in-plane correlation of the nanoparticles) were obtained by integrating the data over the whole length of the PSD (i.e., integrated over the entire range of θ_f or q_z) and plotting the integrated intensities as a function of $q_\parallel$. GIXOS measurements, where scattered intensity is obtained as a function of θ_f or q_z around a fixed ϕ or $q_\parallel$, are sensitive to distribution of electron density in the out-of-plane direction across the surfaces/interfaces. For our measurements, GIXOS data were collected at a fixed in-plane angle ($\phi = 0.3°$ or $q_\parallel = 0.064$ Å^{-1}) using linear PSD, and since data acquisition is relatively faster using this technique, time-dependent studies of structural reordering in transferred monolayers could be performed.

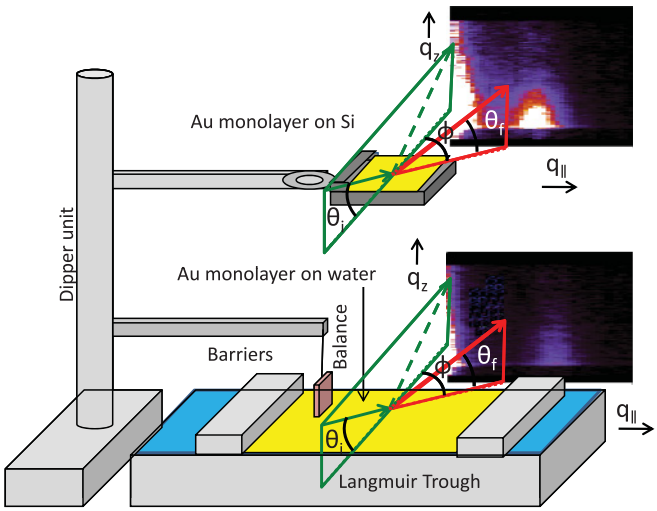

FIG. 1. (Color online) Schematic representation of the experimental setup. Initially, data was collected from the compressed monolayer at air-water interface, and then data was taken from the monolayer transferred on Si substrate as a function of time. Details have been discussed in the text.

III. X-RAY SCATTERING RESULTS

Two-dimensional-scattering profiles and GID plots of selected scattered data collected from monolayer of gold nanoparticles on both water surface and Si substrate as a function of time have been shown in Fig. 2. The peak corresponding to the in-plane correlation between nanoparticles on water surface was found to gradually change its position after transfer of the monolayer to the Si substrate, from $q_\parallel = 0.197 \pm 0.001$ Å^{-1} (after 0.2 h of transfer) to 0.180 ± 0.001 Å^{-1} (after 5 h of transfer). The peak remained stationary immediately after transfer of the monolayer from

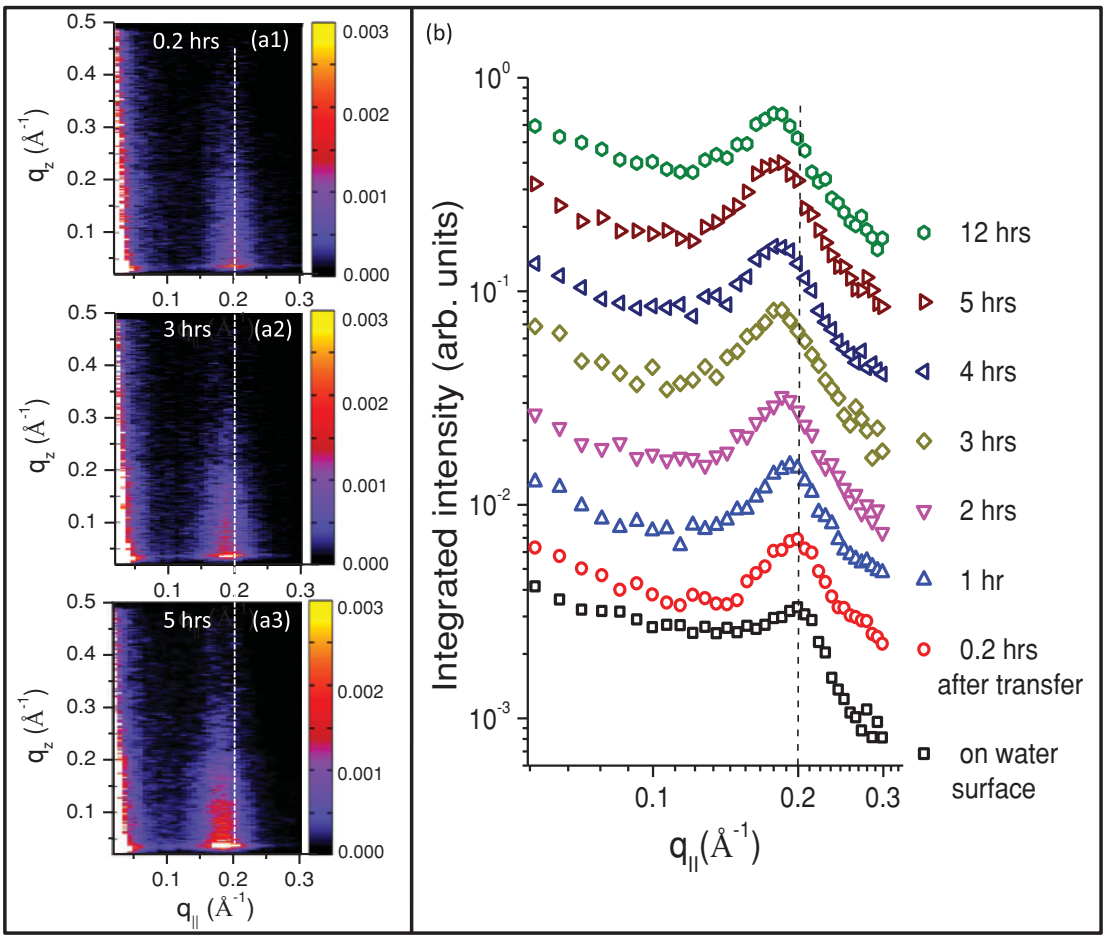

FIG. 2. (Color online) Left panel: (a1)–(a3) Selected 2D x-ray scattering profile of the monolayer of gold nanoparticles on substrate as a function of $q_{\parallel}$ and q_z. Right panel: (b) GID plots obtained from the 2D scattering profiles by integrating the data over q_z. The interparticle correlation peak shifts toward lower $q_{\parallel}$ value and becomes stronger with time.

the water surface to the Si surface for approximately 0.2 h but started shifting toward the lower $q_{\parallel}$ value with time (right panel of Fig. 2).

In general, for any 2D lattice, correlation peaks in the GID plots correspond to the 2D interplanar spacing (d) and appears at $q_{\parallel} = 2\pi/d$. Gold nanoparticles prefer a local hexagonal-closed-pack or triangular (Δ) structure when floating over water as a monolayer [17,18,28]. The interplanar spacing of the nanoparticles on the water surface (d_{liq}) corresponding to the peak position at $q_{\parallel} = 0.197$ Å^{-1} comes out to be 32 Å. The correlation peak position remained fixed for about 0.2 h of transfer (i.e., $d_{\mathrm{liq}} \approx d_{\mathrm{sol}}^{0.2\mathrm{h}}$) but systematic changes were observed at 1, 2, 3, 4, and 5 h. The observed peak, after proper background subtraction [17,28], could be analyzed assuming that it is a superposition of two correlation peaks represented by a pair of Lorentzians. Reasonable fits were obtained by the sum of these Lorentzian functions with fixed centers at 0.197 Å^{-1} (say L1) and 0.180 Å^{-1} (say L2) and a fixed width of 0.1 Å^{-1} (refer to Fig. 3). The GID peaks for the two extreme conditions, namely immediately after transfer and about 5 h after transfer, have also been fitted using a single Lorentzian, and a width of 0.1 Å^{-1} has been obtained for both individually. This width corresponds to a correlation length of 6.3 nm, which is the length scale corresponding to about two nanoparticles. This result clearly indicates a short-range (nearest-neighbor) ordering, signifying that any peak width larger than this peak width (0.1 Å^{-1}) is not physically meaningful here. It is also to be noted that gradual increase (or decrease) in the domain size is not expected as both the extreme phases have only nearest-neighbor ordering. Thus, we have kept the width constant for both the Lorentzians throughout the fitting process. The fits suggest that immediately after transfer, the major contribution to the peak comes from L1 with very small contribution from L2; however, the contribution from L2 increases with time until it is dominant after 5 h of transfer. The factors determining the height of the two Lorentzian functions L1 and L2 are labeled as f_1 and f_2, respectively (refer to Table I for details). After 5 h, the correlation peak (primarily represented by L2) remained stationary at a $q_{\parallel}$ value of 0.180 Å^{-1}, and there was no more observable shift in the peak position even after 12 h. The interplanar spacing of the nanoparticles after 5 h of transfer to Si ($d_{\mathrm{sol}}^{5\mathrm{h}}$) corresponding to the peak position at $q_{\parallel} = 0.180$ Å^{-1} comes out to be 35 Å. Thus, $d_{\mathrm{liq}}/d_{\mathrm{sol}}^{5\mathrm{h}} = 0.91$.

The GIXOS data also show systematic changes as a function of time [refer to Fig. 4(a)]. For the analysis of GIXOS data,

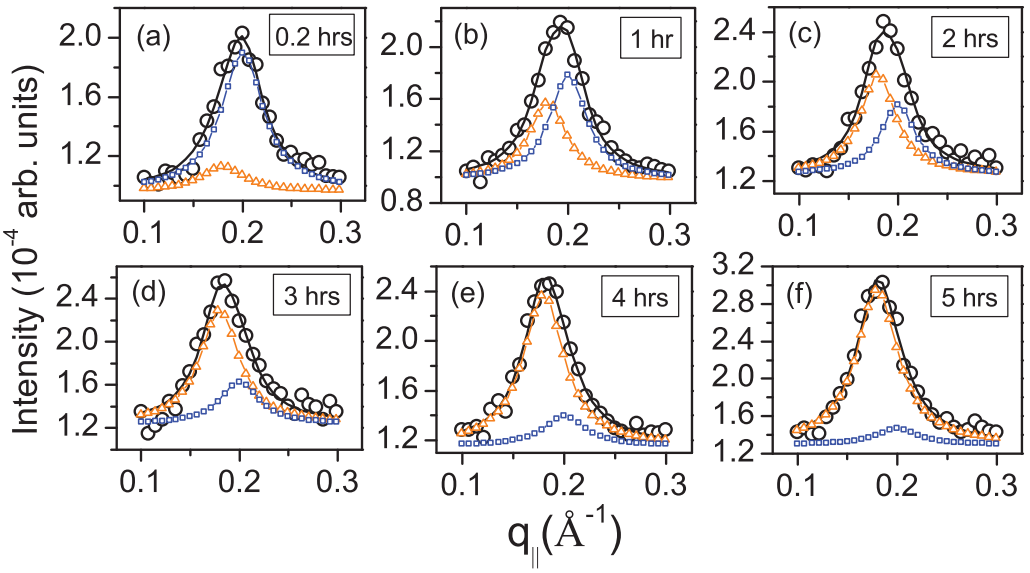

FIG. 3. (Color online) The GID peaks (black open circles) fitted with the sum of a pair of Lorentzians (black solid line) with centers fixed at 0.197 Å^{-1} (L1) and 0.180 Å^{-1} (L2). The contribution to the peak just after transfer from L1 [□ blue (gray) squares and line] is dominant in (a) but with time it becomes weak and the contribution from L2 [Δ orange (light gray) triangles and line] becomes stronger with time (b)–(e) until it is dominant in (f).

we have used the expression for the scattering cross-section (under nonspecular condition), assuming conformality among interfaces [10,35–37] given by

$$\frac{d\sigma}{d\Omega} = \mathcal{A}\mathcal{G}F(q_z)\frac{2\pi}{q_z^2}\left[\frac{e^{-\Gamma_e}}{q_{\max}}\right]^{\eta}\frac{\Gamma(1-\frac{\eta}{2})}{\Gamma(\frac{\eta}{2})}q_{||}^{\eta-2}, \qquad (1)$$

where F(q_z) is given by

$$F(q_z) = \left|\frac{1}{\rho_w}\int\frac{d\rho(z)}{dz}e^{iq_z z}dz\right|^2.$$

$\mathcal{A}$ is the area of scattering volume projected on the surface (determined by the fixed angle of incidence and slits), $\mathcal{G} = r_e^2\rho_w^2|t(\theta_i)|^2|t(\theta_f)|^2\cos^2\phi$ is a geometric function where r_e is classical electron radius, Γ_e (=0.5772) is the Euler constant, the transmission coefficients $t(\theta_i)$ ($t(\theta_f)$) represent the scattering intensity as the incident (scattered) angle approaches the critical angle, the $\cos^2\phi$ term accounts for the beam polarization, and ρ_w is the electron density of water. η is given [36] by $\eta = Bq_z^2/2$ with $B = k_BT/(\pi\gamma)$, where γ is the surface tension and T the temperature. The capillary correlation survives up to at most $q_{\max}$, the maximum wave vector, which is 2π times the reciprocal of the size of the nanoparticle. $\rho(z)$ is the electron density along out-of-plane depth (z).

TABLE I. The factors f_1 and f_2 determining the height of the two Lorentzian functions L1 and L2 used to fit the GID data as described in the text.

Time (h)	0.2	1	2	3	4	5
f_1(10^{-5} arb. units) from L1	0.85	0.58	0.41	0.27	0.17	0.10
f_2(10^{-5} arb. units) from L2	0.15	0.42	0.59	0.73	0.83	0.90

Incidentally, the above formalism works quite well while fitting the GIXOS data of transferred monolayers on Si substrate, hinting at the presence of logarithmic in-plane interfacial correlation (characteristic of capillary waves on liquid surfaces) in the monolayers even after transfer [38]. We have approximated the electron density profile (EDP) ($\rho(z)$) with four stratified layers having finite interfacial roughness over the Si substrate. The four stratified layers are (a) Si native oxide 15 Å, (b) thiol bottom layer 8.8 Å, (c) gold core layer 12.1 Å, and (d) thiol top layer 9.7 Å. The position of the displaced nanoparticles above the lower monolayer has uncertainty in the out-of-plane direction. The AFM results (which shall be discussed later on) show that the percentage of particles in the upper layer (height > 7 nm, excluding buckled positions) is only about 3%. In view of this we have not included any additional upper layer for the GIXOS analysis. In any case, the inclusion of an upper layer almost doubles the thickness of the film and does not represent the observed GIXOS data. The electron density profile of the monolayer changes with time as the monolayer buckles under lateral pressure. The EDPs extracted from the fits of the GIXOS profiles [Fig.4(b)] demonstrate that the monolayer which was initially transferred to the substrate starts restructuring, inducing material movement in the out-of-plane direction as a function of time. The average thickness of the gold core layer increases (so the average thickness of the monolayer increases), but the electron density of the gold core decreases. Such an increment in the thickness of the gold core layer as well as decrement in the electron density of the gold core layer as a function of time happens because the centers of the gold cores are shifted up/down with respect to the nearest neighbors as the monolayer buckles. Similar trends in the EDP have been reported earlier using time-resolved x-ray reflectivity studies on similarly transferred monolayers of gold nanoparticles, and detailed documentation of the model and parameters used to

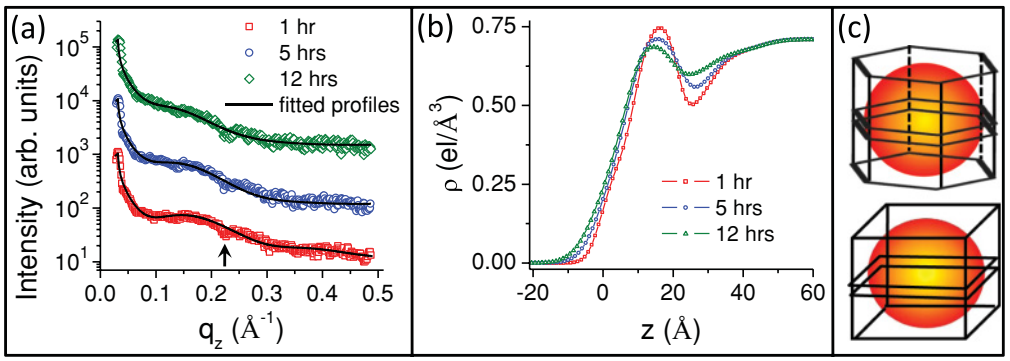

FIG. 4. (Color online) (a) GIXOS profiles (scattered graph) of the monolayer measured as a function of time at fixed $q_\parallel$ value of 0.064 Å^{-1}. Solid lines are corresponding fits. (b) EDP obtained from fitting the GIXOS data. (c) Models used to calculated the EDP of a spherical nanoparticle in Δ and □ packing. The ratio of the observed changes in the EDP of gold nanoparticle in the 1st hour and 5th hour of transfer match well with the calculated EDP for a nanoparticle in Δ and □ arrangements. The dip in all the GIXOS profiles around $q_z = 0.2$ Å^{-1} (marked by arrow) are due to an instrumental problem.

fit the reflectivity data at different surface pressures can be found in Ref. [3]. We have used the same model here for our GIXOS analysis. Now, the ratio of the peak values of the EDP obtained from fitting the GIXOS data [Fig. 4(b)] for the 1st (ρ_{Au}^{1h}) and 5th h (ρ_{Au}^{5h}) EDP profiles comes out to be

$$\frac{\rho_{Au}^{1h}}{\rho_{Au}^{5h}} = 1.049. \quad (2)$$

The intensity of the correlation peak is more toward the low $q_\parallel$ value (left panel of Fig. 2 and also in Fig. 3) due to the form factor $[F(q,R) = \{\sin(qR) - qR\cos(qR)\}/q^3]^2$ of the nanoparticles of radius R [see Fig. 5(a)], which cuts out the peak intensity at higher $q_\parallel$ values.

A simple explanation of the shift in the peak position of the GID profiles (Fig. 2) toward lower $q_\parallel$ value (${q_\parallel}^{1h} > {q_\parallel}^{5h}$) can be dilation of lattice. The decrease in the peak value of electron density ($\rho_{Au}^{1h} > \rho_{Au}^{5h}$) as a function of time, as seen in the EDP extracted from the GIXOS measurements [Fig. 4(b)], also supports the idea of lattice expansion. However, assuming that Δ lattice remains unchanged during this drying process, the ratio of the electron densities as a result of lattice dilation would come out to be

$$\frac{\rho_{Au}^{0.2h}}{\rho_{Au}^{5h}} = \left[\frac{d_{sol}^{5h}}{d_{liq}}\right]^2 = 1.208, \quad (3)$$

but our observed ratio is 1.049, which is much lower [refer to Eq. (2)]. This clearly indicates that dilation in the lattice cannot explain our observation, so an alteration of the lattice that is different from the initial Δ lattice may have to be invoked.

We propose here a model to explain all the x-ray data. This model is also consistent with the microscopy data, which we shall address later on. We assume that the Δ lattice present on the water surface retains the structure until ~0.2 h ($d_{sol}^{0.2h} \sim d_{liq} \equiv d_\Delta$) and undergoes a structural reordering to a □-like lattice within 5 h of transfer ($d_{sol}^{5h} \equiv d_\square$). The observed ratio of d_{liq}/d_{sol}^{5h} is 0.91, which is different from the expected value for the ratio $d_\Delta/d_\square = 0.87$ ($\sqrt{3}/2$) if the nearest-neighbor distance of the nanoparticles remains unchanged. This leads us to infer that the nearest-neighbor distance of the nanoparticles on a water surface having a Δ lattice (a_Δ) is slightly different from the nearest-neighbor distance on the Si surface having a □ lattice ($a_\square$) after 5 h of transfer. Thus,

$$\frac{d_\Delta}{d_\square} = \frac{\sqrt{3}}{2}\frac{a_\Delta}{a_\square} = 0.91, \quad \text{giving} \quad \frac{a_\Delta}{a_\square} = 1.046. \quad (4)$$

The number density (packing fraction) of the particles in a triangular lattice is different from the number density of particles in a square lattice; obviously, the number of particles arranged in a triangular lattice is more than that accommodated in a square lattice. For a gold nanoparticle lattice that reorders from a 2D Δ to a 2D □ arrangement, the expected ratio of the electron density [refer to Fig. 4(c) for models used in the calculation] can be written [using Eq. (4)] as

$$\frac{\rho_\Delta}{\rho_\square} = \frac{\text{Area}_\square}{\text{Area}_\Delta} = \frac{{a_\square}^2}{\frac{\sqrt{3}}{2}{a_\Delta}^2} = 1.05. \quad (5)$$

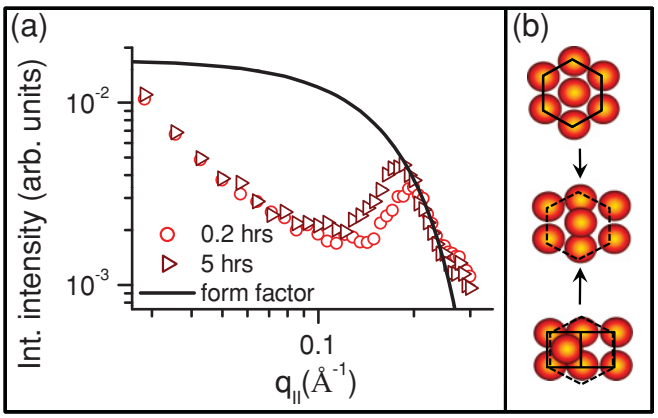

FIG. 5. (Color online) (a) The form factor of the nanoparticles (of radius R) cuts out the peak intensity at higher $q_\parallel$ values. (b) Schematic model representing the initial, intermediate, and final configuration of the nanoparticles in sequential steps, as a result of structural reordering from Δ to □-like lattice. It is to be noted that there is positional uncertainty (in both in-plane as well as out-of-plane direction) in the particle in the upper layer. Refer to text for details.

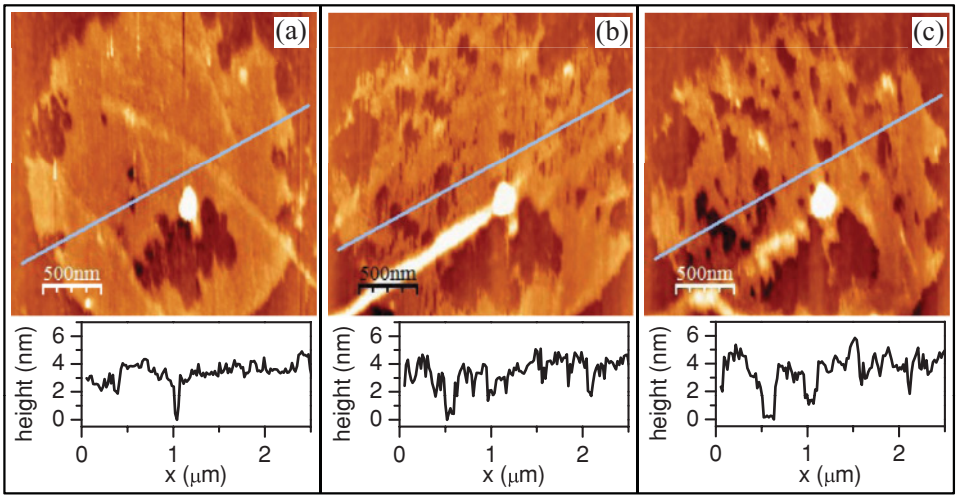

FIG. 6. (Color online) Successive AFM images of the monolayer acquired as a function of time. (a) After 1 hour, (b) after 3 hours, and (c) after 6 hours of transfer. The area occupied by the monolayer on the substrate decreases with time, but the fraction of particles constituting the bilayer increases. Shown below are the typical line profiles of the scans.

Equation (5) is valid for a single particle organized in two Wigner-Seitz cells, corresponding to 2D hexagonal and 2D square phases, respectively. It has been mentioned already that the GIXOS and GID data collected here is insensitive to the upper layer due to its positional uncertainty. Hence Eq. (5) is used here to discuss the packing fraction of the lower monolayer only. This value agrees well with the ratio of the observed peak electron densities obtained from fitting of the GIXOS data [see Eq. (2)]. Besides, the form factor of the nanoparticles, which is responsible for cutting the intensity of the GID peaks at higher $q_{\parallel}$ values [Fig. 5(a)], indicates that only the distances between the nanoparticles have changed as a consequence of structural reorganization.

IV. SUPPORTIVE MICROSCOPY RESULTS

In the scattering experiment, we could not detect any higher-order peaks to prove directly the change in structural symmetry due to the short correlation length of the lattice. A peak corresponding to the in-plane arrangement of the nanoparticles in the second layer could not be detected in the GID measurements, neither could we detect a second layer in the out-of-plane direction using GIXOS measurements. As evident from the model shown in Fig. 5(b), there is positional uncertainty in the displaced upper particle in both in-plane and correspondingly out-of-plane directions. This fact and the lower density of particles in the upper layer are perhaps responsible for not giving any signature of lateral arrangement of the particle in the upper layer. Successive atomic force microscopy (AFM) measurements (NTEGRA Scanning Probe Microscope, NT-MDT), as shown in Fig. 6, were performed on the monolayer after 1 h, 3 h, and 6 h of transfer. The AFM measurements were done in the tapping mode using etched Si_3N_4 cantilevers to minimize tip-induced damages. A large island of gold nanoparticles was seen initially, but after some time, voids started appearing within them which grew in dimension, and at later stages the island assumed a patterned look. From AFM analysis [39], it was observed that the coverage of the monolayer was 76% in the first hour, 67% in the third hour, and 63% in the sixth hour, suggesting compactification (17% shrinkage) in the monolayer. The AFM images also clearly indicated [39] an increment in the fraction of particles constituting the upper layer as a function of time (refer to the line profiles in the lower panels of Fig. 6). Results of systematic AFM measurements were found to be consistent with the results obtained from scattering measurements. The effect of shrinkage in the occupied area can be understood if we assume that initially the nanoparticles in the monolayer were arranged in a hexagonal lattice (having six Δ structures holding 3 nanoparticles on an average), and in about six hours they reorganize into a rectangular structure (formed out of two adjacent $\square$ structures holding 2 nanoparticles on an average and 1 nanoparticle in the upper layer) due to reorganization in the lattice [see schematic in Fig. 5(b)]. The percentage shrinkage in the occupied area then comes out to be $(6 \times \text{Area}_{\Delta} - 2 \times \text{Area}_{\square})/(6 \times \text{Area}_{\Delta}) \times 100 = 15\%$. This value is similar to the observed shrinkage (about 17%) in the monolayer obtained from AFM measurements. However, although the shrinkage in the monolayer during drying could be explained on the basis of our model, direct real-space information of the actual restructuring of the lattice from triangular to square-like lattice could not be achieved in the AFM measurements and we have performed Transmission Electron Microscopy (TEM) measurements to probe the actual restructuring.

Transmission electron microscopy measurements (using a JEOL JEM-2010 microscope operating at 200 kV) were performed on samples to obtain direct real-space evidence of the structural reorganization during the process of drying of the gold nanoparticle monolayer. TEM measurements were performed on two samples deposited on carbon-coated TEM grids, one having a high concentration (0.3 mg/mL) of nanoparticles (in toluene solution) that mimics the compressed phase obtained during transfer of the monolayer from water

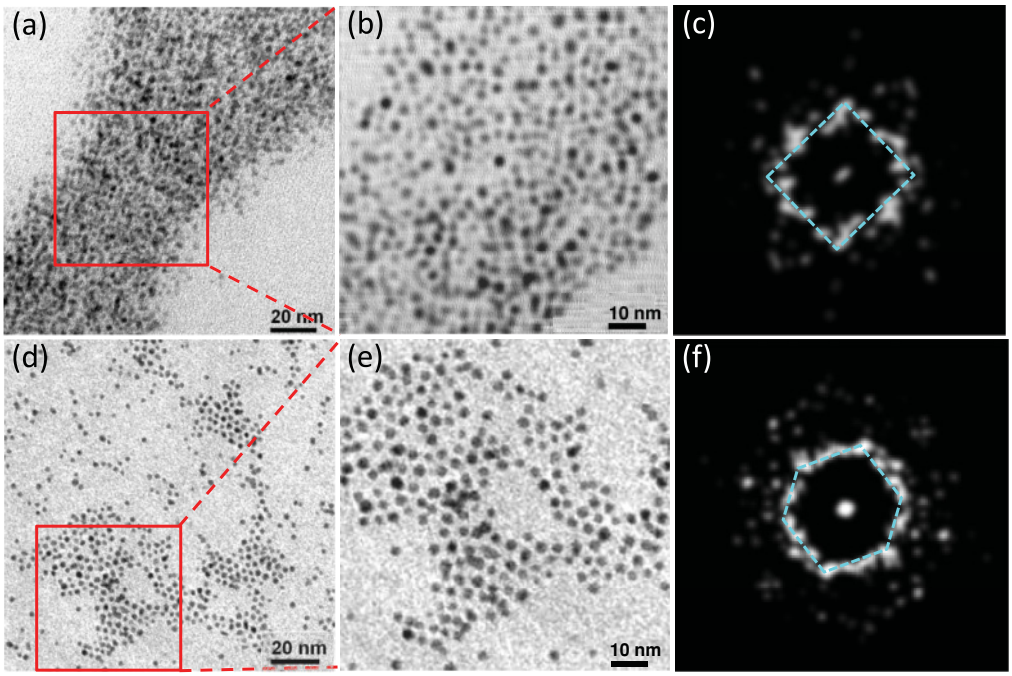

FIG. 7. (Color online) TEM images for two samples on carbon-coated grid. (a) and (b) are for a nanoparticle monolayer with high concentration and mimics the compressed phase obtained during transfer of the monolayer from water surface to solid substrate. Majority of the nanoparticles are in 2D □-like phase. (c) FFT image obtained clearly indicates the 2D □-like phase. (d) and (e) are for a nanoparticle monolayer with very low concentration, which represents a less-compressed phase on water surface. Majority of the nanoparticles are in 2D Δ phase. (f) FFT image indicates a 2D Δ symmetry. The FFT of the images were extracted by using only the coordinates of the nanoparticles to avoid distortion due to differences in shape and size of individual nanoparticles.

surface to solid substrate and the other with a much lower concentration (0.05 mg/mL) of nanoparticles, which represents a less compressed phase on water surface.

The first sample represents a compressed phase obtained after drying and corroborates x-ray findings in showing a predominantly 2D □-like symmetry in the TEM images and the corresponding fast Fourier transform (FFT) [Figs. 7(a)–7(c)], while the second sample shows a predominantly 2D Δ symmetry in the TEM images and the corresponding FFT [Figs. 7(d)–7(f)]. TEM images [Figs. 7(a) and 4(b)] clearly show that during the process of drying the nanoparticles are squeezed between expanding holes. It is further seen that the nanoparticles lose their Δ ordering as a result of such inhomogeneous in-plane pressure and reorganize into a □-like phase as has been obtained in the x-ray scattering results (see Figs. 2, 3, and 4) of the monolayer that goes through the drying process on a solid substrate after transfer from water surface.

V. DISCUSSION

A model that invokes the coexistence of two phases (Δ as well as □-like phase) could explain all the experimental observations, including the observed change in the peak position of interparticle correlation peak in the GID profiles toward a lower $q_{\|}$ value (Fig. 3). Calculations of the expected change in the electron densities of the nanoparticles arranged in Δ (pretransition) and □-like (post-transition) symmetry based on this model matches well with the observed change in the electron densities of the nanoparticles before and after the structural reordering as evidenced in the GIXOS data [Fig. 4(b)]. Supportive microscopy measurements clearly show compactification in the in-plane structure of the transferred monolayer as a function of time. Time-resolved AFM measurements on similarly transferred monolayers indicate shrinkage (refer to Fig. 6) in the coverage area of the monolayer (i.e., particles come closer to each other) continuously after transfer. Compactification in the nanoparticles is also seen in the TEM images of the sample with higher concentration [refer to Figs. 7(a) and 7(b)] of nanoparticles. The FFT results show a □-like symmetry for the sample with higher concentration of nanoparticles [Fig. 7(c)] and presence of a Δ symmetry for the sample with lower concentration of nanoparticles [Fig. 7(f)]. Thus, we see that the model advocating the possibility of structural reordering in the nanoparticle lattice during transfer from water to solid surface seems quite rational and is successful in justifying the observations in GID, GIXOS, as well as supportive microscopy measurements. Existence of a correlation peak with almost unchanged rod profile, even after 5 h of transfer, signifies that short-range order of 2D lattice survives this restructuring. The scattering as well as TEM measurements essentially probe the gold core (gold being a good scatterer) and are rather insensitive to the organic shell. We have assumed that the thiol shell remains unaffected during the drying process.

A monolayer of the colloidal nanosystem is expected to undergo a sequence of structural transition from 1Δ → 1B → 2□, where B is the buckled phase [29–31]. In the model proposed here, we assumed that a 2D structure of the monolayer of gold nanoparticles undergoes similar structural

reordering [refer to the model in Fig. 5(b)]. The 2D Δ or hexagonal ordering gradually assumes a buckled phase and is then rearranged into a 2D □-like ordering as evidenced by the relative intensities of the in-plane correlation peaks at 0.197 $Å^{-1}$ and 0.180 $Å^{-1}$, respectively. The correlation length (domain size) obtained from the width of the fitted Lorentzian corresponding to these peaks remained small and almost unchanged. We observed that immediately after transfer, the major contribution to the peak comes from L1, where the particles are in a 2D Δ ordering with very small contribution from L2, where the particles are in a 2D □ ordering (refer Fig. 3). The fraction of domains corresponding to the Δ symmetry (estimated from value of f_1) were seen to decrease and the fraction of domains corresponding to □ symmetry (estimated from value of f_2) were seen to increase with time until domains corresponding to □ symmetry were dominant with very small contribution from domains corresponding to Δ symmetry after 5 hours of transfer (see Table I). This implies that the small domains of Δ lattice, which were retained in the solid surface immediately after transfer from water surface, undergo a reordering to □-like lattice.

The experimental results and observations based on x-ray scattering, AFM, and TEM measurements suggest that a monolayer of nanoparticles transferred from a liquid surface to a solid surface undergoes a continuous structural reordering from 2D Δ to 2D □-like symmetry during the process of transfer of the monolayer from water to Si surface. All measurements were carried out at room temperature without special arrangements to control or tune the humidity. Since the reorganization essentially is driven by the drying process, slower evaporation rates (expected in a more humid atmosphere) may play an important role is determination of the final structure. However, we have not investigated this aspect here.

VI. CONCLUSION

Time-resolved synchrotron x-ray scattering (viz. GID and GIXOS) measurements were performed to probe the structural reordering in transferred monolayers of gold nanoparticles. The interparticle correlation peak obtained from GID measurements gradually shifted toward lower $q_{\|}$ value with time signifying expansion of lattice. However, GIXOS data and supportive microscopy measurements clearly show compactification in the in-plane structure. The anomaly in the observations could be explained by a model based on the possibility of a 2D short-range structural reordering from Δ to □-like symmetry (via a buckled phase) as a function of time. Detailed analysis of GID peaks support our model of structural reordering in the nanoparticle lattice during transfer from water surface to solid substrate. The change in the observed electron densities of the nanoparticles before and after the structural reordering obtained from fitting of the GIXOS data matches well with the expected change in the calculated electron densities of the nanoparticles arranged in 2D Δ and □ symmetry. TEM and AFM results are found to be consistent with the scattering results. The lateral diffusion processes play an important role in the structural reordering. The lateral pressure generated due to these diffusion processes, which is intimately connected with inhomogeneous drying [3,7], brings about a structural reorganization of the nanoparticles from Δ to □-like symmetry.

ACKNOWLEDGMENTS

R. Banerjee and M. K. Sanyal acknowledge the Department of Science and Technology, India, for funding and support to carry out the experiments at ESRF. We thankfully acknowledge the help of Sangam Banerjee during AFM measurements.

[1] M. Schmidt and H. Löwen, Phys. Rev. Lett. **76**, 4552 (1996).
[2] A. N. Goldstein, C. M. Echer, and A. P. Alivisatos, Science **256**, 1425 (1992).
[3] R. Banerjee, S. Hazra, S. Banerjee, and M. K. Sanyal, Phys. Rev. E **80**, 056204 (2009).
[4] A.-L. Barabási and H. E. Stanley, *Fractal Concepts in surface growth* (Cambridge Univ. Press, Cambridge, 1995).
[5] F. Schreiber, Prog. Surf. Sci. **65**, 151 (2000).
[6] J. N. Israelachivilli, *Intermolecular and Surfaces Forces* (Academic Press, New York, 1992), 2nd ed.
[7] E. Rabani, D. R. Reichman, P. L. Geissler, and L. E. Brus, Nature (London) **426**, 271 (2003).
[8] C. P. Martin, M. O. Blunt, E. Pauliac-Vaujour, A. Stannard, P. Moriarty, I. Vancea, and U. Thiele, Phys. Rev. Lett. **99**, 116103 (2007).
[9] A. Stannard, C. P. Martin, E. Pauliac-Vaujour, P. Moriarty, and U. Thiele, J. Phys. Chem. C **112**, 15195 (2008).
[10] M. K. Bera, M. K. Sanyal, S. Pal, J. Daillant, A. Datta, G. U. Kulkarni, D. Luzet, and O. Konovalov, Europhys. Lett. **78**, 56003 (2007).
[11] R. P. Andres, J. D. Bielefeld, J. I. Henderson, D. B. Janes, V. R. Kolagunta, C. P. Kubiak, W. J. Mahoney, and R. G. Osifchin, Science **273**, 1690 (1996).
[12] J. M. Wessels, H.-G. Nothofer, W. E. Ford, F. v. Wrochem, F. Scholz, T. Vossmeyer, A. Schroedter, H. Weller, and Akio Yasuda, J. Am. Chem. Soc. **126**, 3349 (2004).
[13] S. Pal, M. K. Sanyal, N. S. John, and G. U. Kulkarni, Phys. Rev. B **71**, 121404(R) (2005).
[14] M. A. Garcia, J. de la Venta, P. Crespo, J. LLopis, S. Penadés, A. Fernández, and A. Hernando, Phys. Rev. B **72**, 241403(R) (2005).
[15] Y. Yamamoto, T. Miura, M. Suzuki, N. Kawamura, H. Miyagawa, T. Nakamura, K. Kobayashi, T. Teranishi, and H. Hori, Phys. Rev. Lett. **93**, 116801 (2004).
[16] J. Daillant and M. Alba, Rep. Prog. Phys. **63**, 1725 (2000).
[17] M. Fukuto, R. K. Heilmann, P. S. Pershan, A. Badia, and R. B. Lennox, J. Chem. Phys. **120**, 3446 (2004).
[18] T. A. Weber and F. H. Stillinger, Phys. Rev. E **48**, 4351 (1993).
[19] J. A. Weiss, D. W. Oxtoby, D. G. Grier, and C. A. Murray, J. Chem. Phys. **103**, 1180 (1995).

[20] Y. Han, Y. Shokef, A. M. Alsayed, P. Yunker, T. C. Lubensky, and A. G. Yodh, Nature (London) **456**, 898 (2008).
[21] T. Das, S. Sengupta, and S. Sinha, J. Phys. Condens. Matter **21**, 195408 (2009).
[22] M. J. Stevens, M. O. Robbins, and J. F. Belak, Phys. Rev. Lett. **66**, 3004 (1991).
[23] L. B. Chen, C. F. Zukoski, B. J. Ackerson, H. J. M. Hanley, G. C. Straty, J. Barker, and C. J. Glinka, Phys. Rev. Lett. **69**, 688 (1992).
[24] W. Wen, N. Wang, H. Ma, Z. Lin, W. Y. Tam, C. T. Chan, and P. Sheng, Phys. Rev. Lett. **82**, 4248 (1999).
[25] A. Chaudhuri, S. Sengupta, and M. Rao, Phys. Rev. Lett. **95**, 266103 (2005).
[26] A. Sengupta, S. Sengupta, and G. I. Menon, Phys. Rev. B **75**, 180201(R) (2007).
[27] Y. K. Koh and C. C. Wong, Langmuir **22**, 897 (2006).
[28] D. Pontoni, K. J. Alvine, A. Checco, O. Gang, B. M. Ocko, and P. S. Pershan, Phys. Rev. Lett. **102**, 016101 (2009).
[29] P. Pieranski, L. Strzelecki, and B. Pansu, Phys. Rev. Lett. **50**, 900 (1983).
[30] S. Neser, C. Bechinger, P. Leiderer, and T. Palberg, Phys. Rev. Lett. **79**, 2348 (1997).
[31] F. Ramiro-Manzano, E. Bonet, I. Rodriguez, and F. Meseguer, Phys. Rev. E **76**, 050401(R) (2007).
[32] M. Brust, M. Walker, D. Bethell, D. J. Schiffrin, and R. Whyman, J. Chem. Soc. Chem. Commun. 801 (1994).
[33] A. Datta, S. Kundu, M. K. Sanyal, J. Daillant, D. D. Luzet, C. Blot, and B. Struth, Phys. Rev. E **71**, 041604 (2005).
[34] M. Tolan, *X-Ray Scattering from Soft-Matter Thin Films* (Springer, Berlin, 1999); *X-Ray and Neutron Reflectivity: Principles and Applications*, edited by J. Daillant and A. Gibaud (Springer, Paris, 1999).
[35] S. Mora, J. Daillant, K. Mecke, D. Luzet, A. Braslau, M. Alba, and B. Struth, Phys. Rev. Lett. **90**, 216101 (2003).
[36] M. K. Sanyal, S. K. Sinha, K. G. Huang, and B. M. Ocko, Phys. Rev. Lett. **66**, 628 (1991).
[37] J. K. Basu and M. K. Sanyal, Phys. Rep. **363**, 1 (2002).
[38] J. K. Basu and M. K. Sanyal, Phys. Rev. Lett. **79**, 4617 (1997).
[39] I. Horcas, R. Fernández, J. M. Gómez-Rodriguez, J. Colchero, J. Gómez-Herrero, and A. M. Baro, Rev. Sci. Instrum. **78**, 013705 (2007).